Effect of Solvent Quality on the Phase Behavior of Polyelectrolyte Complexes

Lu Li,[1] Artem M. Rumyantsev,[1] Samanvaya Srivastava,[2,*] Siqi Meng,[1] Juan J. de Pablo[1,3,*] and Matthew V. Tirrell[1,3,*]

[1]Pritzker School of Molecular Engineering, The University of Chicago, Chicago, IL 60637, USA
[2]Chemical and Biomolecular Engineering, University of California, Los Angeles, Los Angeles, CA 90095, USA
[3]Center for Molecular Engineering and Materials Science Division, Argonne National Laboratory, Lemont, IL 60439, USA

KEYWORDS: Polyelectrolyte complexation, Phase Behavior, Hydrophobicity, RPA Theory

ABSTRACT: The role of polyelectrolyte-solvent interactions, among other non-Coulomb interactions, in dictating the thermodynamics and kinetics of polyelectrolyte complexation is prominent, yet sparingly studied. In this article, we present systematic comparisons of the binodal phase behavior of polyelectrolyte complexes (PECs) comprising polyelectrolytes with varying quality of backbone-solvent interactions. Experimental phase diagrams of polyelectrolyte complexes with either a peptide or an aliphatic backbone highlight the influence of backbone chemistry on the composition of complexes and their salt resistance. Corresponding theoretical phase diagrams, obtained from a framework combining the random phase approximation and Flory-Huggins approach, reveal a transition from closed phase boundaries with confined two-phase regions for PECs in good solvents to open phase boundaries, wherein two-phase systems are predicted to exist even at very high salt concentrations, for PECs in poor solvents. These predictions compare fittingly with experimental observations of low salt resistance (~1 M NaCl) of PECs comprising hydrophilic polyelectrolytes and persistence of complexes, stabilized by short-range hydrophobic interactions, even at very high salt concentrations (~6 M NaCl) for PECs comprising hydrophobic polyelectrolytes.

I. INTRODUCTION

Polyelectrolyte complexes (PECs) have garnered recent interest as model systems for gene delivery vehicles,[1–4] bioadhesives[5,6] and membraneless organelle mimics.[7,8] An increasing number of investigations have focused on thermodynamics,[9–11] morphology,[12–17] and mechanical properties[18–21] of PECs comprising biologically-derived[22–24] as well as synthetic[12,15,21,25,26] polyelectrolytes. Experiments,[9–11] theory,[27–30] and computer simulations[31–33] have shown that complexation proceeds by associative phase separation of oppositely charged polyelectrolytes in aqueous solutions driven by cooperative electrostatic interactions and entropy of counterion release.[34–37] Correspondingly, the effects of polyelectrolyte molecular weights, architectures, charge densities, mixing ratio, and solution conditions including pH, salt concentration, and temperature on PEC characteristics have been detailed extensively.[12,15,25,30,38–45]

Inter-polyelectrolyte and polyelectrolyte-solvent interaction,[20,38,46,47] even while being acknowledged in early treatments[48–50] to influence thermodynamics and kinetics of complexation, have received relatively scant attention. This can be ascribed primarily to a lack of polyelectrolyte systems that facilitate systematic and comprehensive examination of the interplay of electrostatic and hydrophobic interactions in solution. Contemporary efforts have incorporated an *ad hoc* Flory-Huggins χ parameter in the classic Voorn-Overbeek theory of polyelectrolyte complexation[48] to model the phase behavior and salt stability of PECs.[26,34,47] More recently, a systematic investigation of the effect of hydrophobicity of the functional groups of poly(4-vinylpyridine), quaternized with methyl, ethyl, and propyl substituents, on the PEC stability, rheology and swelling characteristics was discussed by Sadman *et al.*, showing increasing salt resistance with longer alkyl chains.[20] However, these reports primarily focused on evaluating the influence of charged functional side groups on the physical attributes of the complexes; the role of the polymeric backbone in dictating PEC characteristics remain to be clarified.

With the insights drawn from our previous investigations[10,12,13] and a companion paper that discusses the phase behavior of oppositely charged polyelectrolytes with hydrophobic backbones,[51] we employ polyelectrolytes with peptide and aliphatic backbones, but with side groups having identical functionality, to investigate quantitatively the effect of backbone chemistry on PEC phase behavior. The polyelectrolytes - poly(L-lysine hydrochloride) (PLK), poly(D,L-glutamic acid sodium salt) (PRE), poly(allylamine hydrochloride) (PAH), and poly(acrylic acid sodium salt) (PAA) were accompanied by sodium or chloride counterions. Composition maps of mixtures of polycation, polyanion, sodium chloride and water were elucidated through thermogravimetric analysis. The strength of electrostatic interactions and entropy contributions within four polyelectrolyte pairs were expected to be similar; the major differences of their phase behaviors were anticipated to originate from polyelectrolyte backbone interactions. Interpretation of the experimental data was facilitated by comparisons with predictions from theoretical analysis based on the random phase approximation (RPA) theory and Flory-

Huggins lattice model with predictive capabilities. Incorporation of a physical theory allowed for a clear isolation of a single parameter to describe polyelectrolyte-polyelectrolyte and polyelectrolyte-solvent interactions, corroborating the conclusions drawn from experiments.

II. EXPERIMENTAL AND THEORETICAL METHODS

Materials and Preparation of Stock Solution. Poly(L-lysine hydrochloride) (PLK, degree of polymerization N = 100, molecular weight = 16000 g/mol) and poly(D,L-glutamic acid sodium salt) (PRE, N = 100, molecular weight = 15,000 g/mol) were purchased from Alamanda Polymers (Huntsville, AL USA). Poly(acrylic acid sodium salt) (PAANa, N = 158, molecular weight = 14800 g/mol) was purchased from Polymer Source Inc. (Dorval, Canada). Poly(allylamine hydrochloride) (PAH, N = 160, molecular weight = 15,000 g/mol) was purchased from AK Scientific Inc. (Union City, CA USA). Sodium chloride (NaCl, ACS grade) was purchased from Millipore Sigma (St. Louis, MO). All chemicals were used without further purification. 10% wt/v stock polyelectrolyte solutions in MilliQ™ water were prepared and vortexed for 1 minute. The polypeptide stock solutions were sonicated for 30 minutes as per manufacturer's instructions to obtain clear solutions, and the PAA and PAH stock solutions were sonicated for 6 hours to fully dissolve the polymers for clear solutions. 5 and 6 M NaCl stock solutions were prepared for further sample preparation.

Preparation of Polyelectrolyte Complexes. Polyelectrolyte complexes were prepared by mixing polyelectrolyte stock solutions, NaCl stock solution and water in appropriate ratios to achieve desired total polyelectrolyte concentration ($\phi_{P,0}$) and added salt concentration (Λ_S) while maintaining 1:1 stoichiometric ratio of polyelectrolyte charge. The required amounts of chosen polycation stock solutions were added to a solution containing the desired amounts of MilliQ™ water and NaCl stock solution (5 M) in a 1.5 mL Eppendorf tube and vortexed for 30 sec. Next, the required amounts of chosen polyanion stock solutions were added, and the solution mixtures were vortexed again for 30 sec. Four pairs of polyelectrolyte complexation systems with varying degrees of hydrophobicity were investigated: PAA with PAH, PAA with PLK, PRE with PAH, and PRE with PLK.

Salt Resistance Measurements by Microscopy. The added salt concentrations required for complete dissolution of PECs, referred to as the salt resistance (Λ_S^*) of the PECs, were determined by phase contrast optical microscopy (Leica DMI 6000B) of the PEC samples prepared at total polyelectrolyte concentrations $\phi_{P,0} = 1\%\, wt/v$ with varying added salt concentrations (Λ_S). 200 µl of solution mixtures prepared as described above were placed in ultra-low attachment 96-well plates (Costar, Corning Inc.) for microscopic imaging. Morphological transitions from phase-separated complexes to one homogenous phase were recorded with increased concentration of added salt.

Thermogravimetric Analysis. 1.5 mL Eppendorf tubes containing 300 to 1000µl samples were centrifuged at 17000g for 15 min. 30 µL of the supernatant and an appropriate amount of the complex were extracted, transferred into separate aluminum pans, and placed in Barnstead Thermolyne Furnace 1400 to for thermal processing. The operating atmosphere in the furnace was air. The following thermal processing protocol was used: samples were heated from room temperature to 110 °C and held for 2.5 h. Samples were subsequently cooled to room temperature, weighed to estimate weight loss corresponding to the water content. The samples were returned to the furnace and heated to 600 °C. After heating for 12 h, the samples were cooled to room temperature, and their weights were measured again to estimate the polymer and salt contents. At least 3 repeats were conducted for each PEC sample with prescribed total polyelectrolyte concentration ($\phi_{P,0}$) and added salt concentration (Λ_S). The weight fractions of water, polymer, and salt were recorded and converted to volume fractions ϕ_P, ϕ_S and ϕ_W , respectively, by assuming same density of polymer and salt in bulk and solution state. Densities $\rho_{PLK-PRE}$ = 1.2515 g/mL, $\rho_{PPAH-PAA}$= 1.3308 g/mL, $\rho_{PLK-PAA}$= 1.3217 g/mL, $\rho_{PAH-PRE}$= 1.3033 g/mL, ρ_{salt}= 2.16 g/mL, and ρ_{water} = 1.00 g/mL were used. Statistical analysis using Dixon's Q test was performed for the identification and rejection of outliers.

Theoretical Considerations. We considered the theoretical situation of stoichiometrically equivalent solutions of oppositely charged polyelectrolytes (polycation and polyanion volume fractions $\phi_+ = \phi_-$) capable of forming a complex phase coexisting with a dilute supernatant. Polycations and polyanions had equal statistical segment sizes a , equal number of segments, $N_+ = N_- = N$, and contained equal fractions of ionic monomers, $f_+ = f_- = f$, each carrying quenched charge $\pm e$. We focused on weakly charged polyions, $f \ll 1$, which form complexes of low polymer density. Due to low polyelectrolyte volume fraction $\phi = 2\phi_+ = 2\phi_-$ within the complex, $\phi \ll 1$, dielectric constants of the complex and supernatant phases were assumed to be equal to that of the solvent, ϵ . The dimensionless Bjerrum length is $u = l_b/a = e^2/\epsilon a k_B T$. In aqueous solutions, where l_b = 0.7 nm and $u \approx 1$, effects of cross-chain ion pairing within the complex are negligible.[52,53] Salt concentration c_S was considered to be the number of cations and anions per a^3 volume. The free energy of the solution and its volume were denoted by $\mathcal{F}$ and V , respectively.

Binodal phase boundaries of the solution were determined by estimating the free energy density F expressed in $k_B T/a^3$ units, $F = \mathcal{F}a^3/Vk_B T$, as the sum of three contributions

$$F = F_{corr} + F_{tr} + F_{FH} \quad (1)$$

The first and the second terms, F_{corr} and F_{tr}, describe the Coulombic interactions between all the charged species (polyelectrolytes and salt ions) and translational entropy of

salt ions, respectively. The third term F_{FH}, expressed in the framework of the Flory-Huggins (FH) lattice model, is the free energy of the salt-free solution of the corresponding neutral polymers. In the mean-field (saddle-point) approximation, the free energy of electrostatic interactions is zero owing to the system being charge neutral. Coulombic attraction between polyions therefore arise from fluctuations (correlations) and were treated using the random phase approximation (RPA) formalism.[27,53–60] The corresponding free energy density can be expressed as[54,60–62]

$$F_{corr} = \frac{1}{12\pi\left(r_p/a\right)^3}(1-s)\sqrt{2+s} \tag{2}$$

The parameter s is the reduced salt concentration, $s = \left(r_p/r_D\right)^2$, equal to the squared ratio between the screening radius by polymer, $r_p/\mathrm{a} = (48\pi u f^2\phi)^{-1/4}$, and the Debye screening length, $r_D/a = (4\pi u c_s)^{-1/2}$. Equation 2 implies that salt ions are considered as point-like charges, so that their translational entropy has an ideal-gas form

$$F_{tr} = c_S \ln c_s \tag{3}$$

The FH term, F_{FH}, incorporates the translational entropy of polyelectrolytes and solvent (water) as well as the short-range pairwise interactions between the polyelectrolytes and the solvent. The latter was written as $\chi_{+w}\phi_+\phi_w + \chi_{-w}\phi_-\phi_w + \chi_{+-}\phi_+\phi_-$. Here χ_{+w}, χ_{-w} and χ_{+-} denote the interaction parameters between polycation monomers and solvent, polyanion monomers and solvent, and polycation and polyanion monomers, respectively. The solvent volume fraction $\phi_w = 1-\phi$; salt ions were assumed to be point-like and do not contribute any volume to the system. Thus, an effective FH parameter of interaction χ between the polyelectrolyte pair and the solvent were defined as[62]

$$\chi = \frac{\chi_{+w}+\chi_{-w}}{2} - \frac{\chi_{+-}}{4} \tag{4}$$

Omitting linear ϕ terms, F_{FH} can therefore be written as

$$F_{FH} = \frac{\phi}{N}\ln\frac{\phi}{2} + (1-\phi)\ln(1-\phi) - \chi\phi^2 \tag{5}$$

It could be argued that the effective solvent quality for the complex phase decreases when it decreases for each of the polyions, i.e., χ is the increasing function of χ_{+w} and χ_{-w}. However, immiscibility of the polyions with each other, resulting from short-range repulsions between polyanions and polycations, can favor swelling of the complexes.[62] At the same time, when the uncharged monomers of the oppositely charged polyelectrolytes are compatible, $\chi_{+-} \approx 0$, then the effective solvent quality for the complex phase can be approximated equal to the average of those for polyanion and polycation, $\chi = (\chi_{+w}+\chi_{-w})/2$.

Binodal phase boundaries of the solution are defined by the equality of the osmotic pressures, Π, as well as salt and polymer chemical potentials, μ_s and μ_p, in the coexisting phases

$$\begin{cases} \Pi\left(\phi^{\mathrm{comp}}, \mathrm{c_s^{comp}}\right) = \Pi\left(\phi^{\mathrm{sup}}, \mathrm{c_s^{sup}}\right) \\ \mu_{\mathrm{s}}\left(\phi^{\mathrm{comp}}, \mathrm{c_s^{comp}}\right) = \mu_{\mathrm{s}}\left(\phi^{\mathrm{sup}}, \mathrm{c_s^{sup}}\right) \\ \mu_{\mathrm{p}}\left(\phi^{\mathrm{comp}}, \mathrm{c_s^{comp}}\right) = \mu_{\mathrm{p}}\left(\phi^{\mathrm{sup}}, \mathrm{c_s^{sup}}\right) \end{cases} \tag{6}$$

Chemical potentials are given by $\mu_s = \partial F/\partial c_s$ and $\mu_p = \partial F/\partial\phi_P$. Accordingly, the osmotic pressure can be calculated as $\Pi = c_s\mu_s + \phi\mu_p - F$. The effect of hydrophobicity of polyion backbones on the complexation phenomenon was investigated by determining the binodal phase boundaries obtained from the numerical solution of the set of Equations 6 for different effective solvent qualities ranging between $\chi = 0.4$ (moderately good solvent) and $\chi = 0.6$ (moderately poor solvent). Note that at $\chi = 0.4$, solvent is good, but the deviation from the Θ point, $\chi = 0.5$, is low, so that the statistics of the polyelectrolytes within the complex phase could be considered Gaussian, even at small length scales.[61] In this case, Equation 2 which was derived under the assumption that the polyelectrolytes within the complex phase have ideal-coil conformations, is applicable.[61]

The RPA correlation correction is inaccurate at very low polymer concentrations.[63–65] Detailed analysis[63,66] shows that polyanions and polycations in supernatant (where polymer concentration is low) can form finite size complex aggregates; this fact is disregarded in our theoretical model. Nevertheless, fully-fluctuating field-theoretic simulations[63–65] have shown that the predictions of the RPA on the density of the complex phase are highly reliable in the entire range of salt concentrations, except the vicinity of the critical point where mean-field theories generally break down.[67]

To ensure consistency and rigorous accuracy of our theoretical considerations (at least in the treatment of the complex phase), we restricted our analysis to the case of weakly charged chains, $f \ll 1$.[36,62] We noted the mismatch of this charge density regime with our experimental studies where the polyelectrolytes studied have high charge densities. However, the proposed theoretical model is able to account for the trends in the solution phase behavior, including the effect of the polyions hydrophobicity on the stability of the complexes. To develop the quantitative theory of the described phenomena, which would be applicable at $f \simeq 1$, readers may refer to transfer matrix formalism,[68] liquid state theory approaches,[30,69–71] and field-theoretic simulations.[63–65] It must also be noted that all thermodynamic theories, including the formalism considered here, are applicable to equilibrium liquid complexes but not to solid complexes which may exist in kinetically arrested states.[72,73]

III. RESULTS AND DISCUSSION

III.1 Effect of Polyelectrolyte Length on Phase Behavior of Complexes: Model Validation

Length of polyelectrolyte chains is known to influence the composition of complexes they form. Polyelectrolyte content and the height of the two-phase window both increase with increasing lengths, although the trends approach a plateau for long polyelectrolytes. Our previous investigations on phase

behavior of length-matched charge-matched PLK-PRE complexes highlighted these trends.[12] Polyelectrolyte volume fraction of the complexes, ϕ_P, increased prominently upon increasing chains lengths from 20-mers to 50-mers. Increasing chain lengths from 50-mers to 100-mers to 400-mers, however, did not produce distinguishable increases in ϕ_P, particularly in the low salt volume fraction, ϕ_S, regime (**Figure S1**).[12] On the contrary, height of the two-phase window, a proxy for the salt resistance of the complexes, increased continually with longer chain lengths.[12]

Binodal phase envelope predictions for mixtures of oppositely charged polyelectrolytes of varying lengths and fraction of ionic units $f = 0.1$ in an effective Θ-solvent ($\chi = 0.5$) with dimensionless Bjerrum length $u = 1$ are shown in **Figure 1**. Evolution of the phase boundaries with N followed expected trends; ϕ increased with N in the range of $100 \leq N \leq 400$ before plateauing for $400 \leq N \leq 1600$. The vanishing translational entropy term as $N \to \infty$ in Equation 5 led to the saturation of the salt-free complex density as N increases, in accordance with our previously published experimental data[12] shown in **Figure S1**. However, salt concentration at critical point c_S^{cr}, an indicator of the height of the two-phase window, increased with N continually, in agreement with our previous results[12] and trends reported in the literature.[21,74]

The inset in **Figure 1** shows the salt concentration at critical point c_s^{cr}, obtained within the framework of the RPA considerations, increasing with N, along with the limiting scaling law $c_s^{cr} \sim N^{1/2}$ being valid for sufficiently long chains ($N \gtrsim 500$ for the chosen values of parameters). The scaling

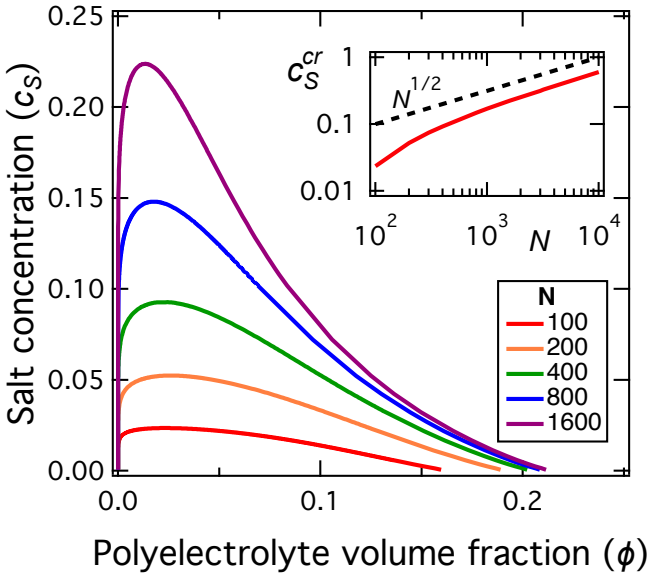

Figure 1. Polymer volume fraction (ϕ)-salt concentration (c_S) representation of the theoretical predictions of the binodal phase boundaries of solutions comprising polyelectrolytes of varying lengths, N. Curves are plotted for $f = 0.1$, $\chi = 0.5$ (Θ solvent), and $u = 1$. ***Inset***: Log-log dependence of the salt concentration at the critical point on the length of the polyions, $c_S^{cr}(N)$. At high N values, $c_S^{cr} \sim N^{1/2}$, in accordance with the scaling estimates (dashed line).

predictions could be obtained by arguing that polyelectrolytes in Θ solvents adopt ideal-coil conformations at all length scales. Thus, the correlation length (blob size) within the complex is $\xi \simeq \phi^{-1} \simeq c_s/f^2$, using the predictions of $\phi \simeq f^2/c_s$ for polyelectrolyte complexes containing high salt concentrations.[54,61,75] The complex phase can be envisioned to be composed of densely packed oppositely charged blobs, each of the size ξ and containing $g \simeq \xi^2 \simeq c_s^2/f^4$ monomers. A positively charged blob is preferably surrounded by negatively charged blobs, and the energy of Coulomb attraction is of the same order as thermal energy, k_BT, per blob.[61] For long polyelectrolyte chains, $N \gg g$, free energy gain per chain due to complexation far exceeds k_BT, and associative phase separation is thermodynamically favorable. However, as g approaches N, Coulomb attraction between the chains scales as k_BT per chain and becomes too weak to overcome their translational entropy. Neglecting numerical factors, salt concentration at the critical point can therefore be estimate as $c_s^{cr} \simeq N^{1/2}f^2 \sim N^{1/2}$, in agreement with the accurate RPA results shown in the inset of **Figure 1**. It must be noted that this result is limited to the range of applicability of RPA theory, $c_s \ll 1$.[61] Further, experimentally observed growth of c_S^{cr} with N is weaker than $N^{1/2}$, and can be ascribed to water being a good rather than a Θ solvent for the polypeptide chains. Nevertheless, the qualitative similarities between theoretical predictions and experimental trends endorse the capability of the theoretical framework to capture the essential physics of polyelectrolyte complexation and enable concurrent theoretical and experimental investigations of the effect of solvent quality on the complexation phenomena.

III.2 Effect of Polyelectrolyte Backbone Hydrophobicity on Phase Behavior of Complexes

Figure 2a displays optical micrographs depicting the morphological transitions of the complexes upon mixing polyelectrolyte pairs PAH-PAA,[43] PLK-PAA, PAH-PRE, and PLK-PRE[12,76] systems with total polyelectrolyte concentration $\phi_{P,0} = 1\%\ wt/v$ (i) in absence of any added salt ($\Lambda_S = 0$), and at (ii) low and (iii) high concentrations of added salt (Λ_S). PLK and PRE have hydrophilic backbones comprising peptide linkages, while PAH and PAA possess hydrophobic aliphatic backbones (chemical structures of the four polyelectrolytes are shown by **Figure 2b**). As illustrated in the micrographs, complexes comprising hydrophilic polyelectrolyte pair (PLK and PRE) existed as liquid coacervate droplets owning to their high water content, and complexation was completely suppressed upon exceeding the salt resistance (Λ_S^* =1.025 M, **Figure 2c**).[12,76] On the contrary, in complexes comprising hydrophobic polyelectrolytes (PAH and PAA), amorphous precipitates formed at low added salt concentrations that transitioned to semi-solid soft structures to fluid droplets upon increasing addition of salt. It must be noted that complete dissolution of the PAH-PAA complexes was not observed in as high as 6 M salt concentration in solutions; salt

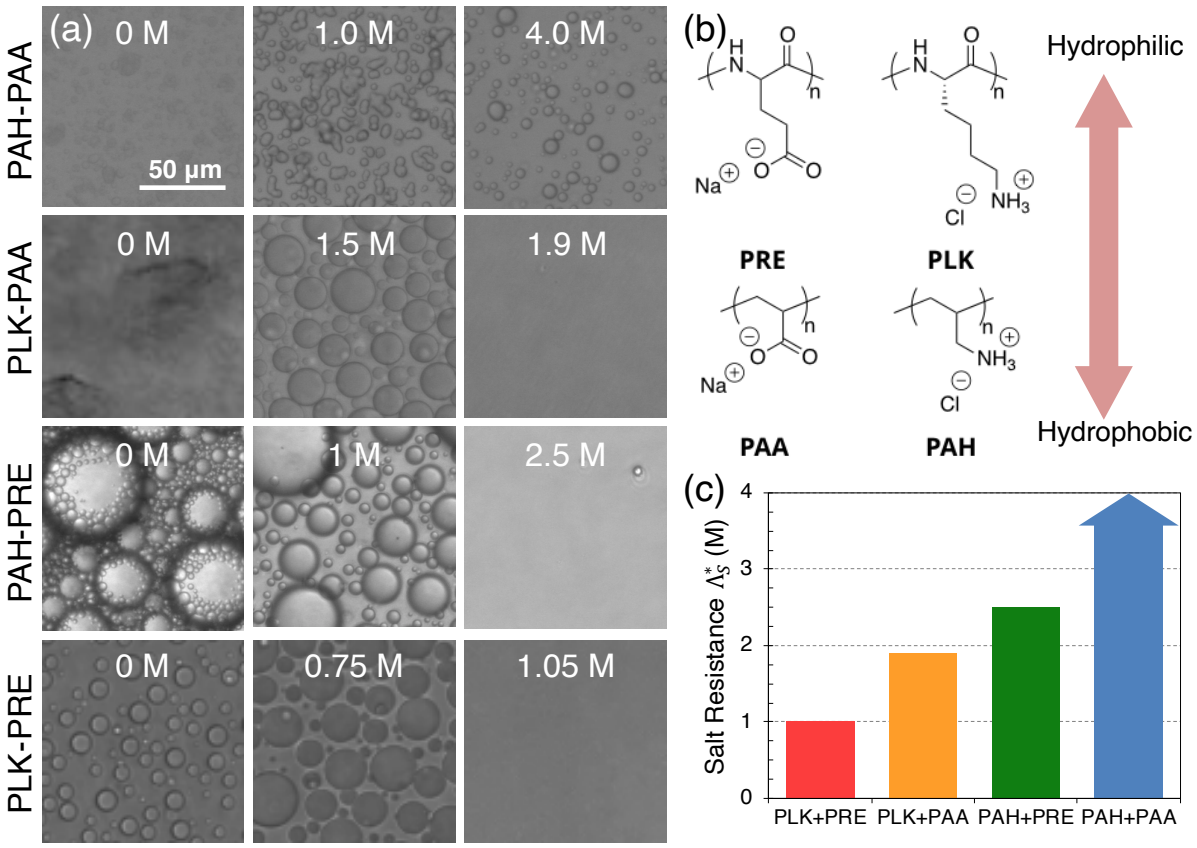

Figure 2. Stabilities of complexes in salt containing environments. (a) Microscopic representatives of the phase separated complexation systems with varying degrees of hydrophobicity. PAH-PAA, the most hydrophobic pair, showed gel-like semi-solid aggregates. PLK-PRE, the most hydrophilic pair, showed liquid droplets. PLK-PAA and PAH-PRE, the intermediate pairs, showed transitional behaviors. (b) Chemical structures of polyelectrolytes employed. (c) NaCl salt resistance for the PECs comprising the respective polyelectrolyte pairs. PAH-PAA complexes did not dissolve even at the highest NaCl concentration (6 M) investigated.

resistance of PAH-PAA complexes exceeded the solubility of NaCl in water at room temperature.[44,47]

The morphology and response to addition of salt of complexes comprising polyelectrolytes with hydrophilic and hydrophobic backbones were expected to be between the trends observed for the hydrophobic- hydrophobic pair and the hydrophilic-hydrophilic pair of polyelectrolytes. PLK-PAA complexes were found to be flaky precipitates in the absence of added salt, transitioned to liquid droplets upon addition of salt before completely dissolving at Λ_S^* =1.9 M (**Figure 2c**). PAH-PRE formed liquid coacervate droplets, albeit with a distinct morphology in the absence of added salt. The first image in the third row of **Figure 2a** shows small satellite droplets resting around and on top of primary coacervate droplets. We hypothesize that the diffusion of the smaller satellite droplets inside large primary droplets were remarkably hindered, resulting in the formation of inhomogeneous assemblies. Upon addition of salt, the droplets became homogenous, before dissolving completely at Λ_S^* = 2.5 M (**Figure 2c**). However, the formation of inhomogeneous liquid droplets in the PAH-PRE complexes in the absence of added salt was an unexpected observation.

Composition of the complex and supernatant phases obtained upon mixing oppositely charged polyelectrolytes with total polyelectrolyte concentration ($\phi_{P,0}$) and added salt concentration (Λ_S) are depicted in detailed binodal polymer concentration (ϕ_P) – salt concentration (ϕ_S) maps in **Figure 3**. Among the four polyelectrolyte-pairs, backbones of the PLK-PRE and PAH-PAA represent the two extremes of the hydrophilic-hydrophobic backbone spectrum. Correspondingly, compositions of the complex and the supernatant phase, as deduced from thermogravimetric analysis, evolved distinctively for these systems with varying $\phi_{P,0}$ and Λ_S in solution. Polymer content in the complex phases (depicted by the right branch of the binodal phase boundaries) formed by the polypeptide PLK-PRE pair was generally less than those formed by the PAH-PAA pair with aliphatic backbones. Further, on the ϕ_P-ϕ_S plane, the two branches representing the complex and supernatant phases merged into one for the PLK-PRE pair, indicating complete suppression of complexation irrespective of the total polymer concentration and a one-phase region for all ϕ_P values beyond a critical ϕ_S value. However, merging of the two branches representing the complex and supernatant phases was not observed for the PAH-PAA pair, and the polymer-

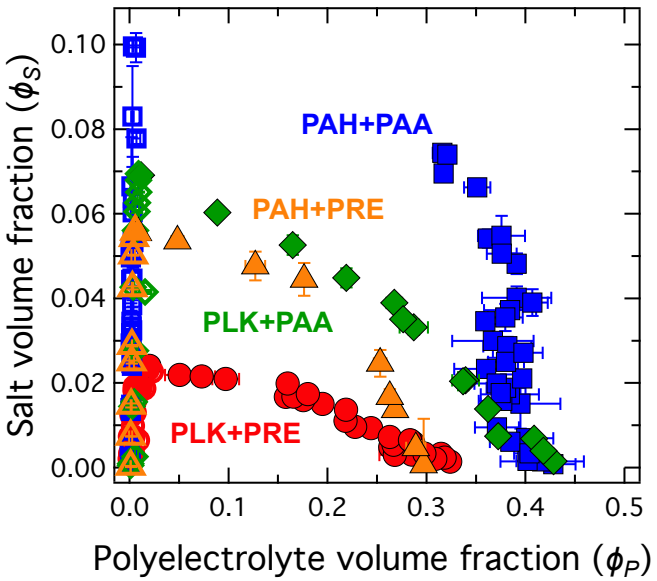

Figure 3. Binodal phase diagrams of different PEC systems. The binodal composition data were plotted in salt volume fraction (ϕ_S)-polymer volume fraction (ϕ_P) map. The solid (complex phase) and open (supernatant phase) blue squares, green diamonds, orange triangles, and red circles were the results obtained from TGA measurements for PAH-PAA, PAH-PRE, PLK-PAA, and PLK-PRE pairs. The overall shapes of the binodal phase boundaries evolved from an open form of the most hydrophobic PAH-PAA complexes to a closed form for complexes containing at least one hydrophilic polyelectrolyte.

rich phases that formed upon complexation were able to tolerate high concentrations of salt. Relatedly, ϕ_P in the complex phase decreased drastically upon addition of salt in the system composed of polypeptides, but the variations of ϕ_P with increasing amounts of added salt were suppressed, and even non-monotonic at low added salt concentrations, for the systems composed of aliphatic polyelectrolytes. For example, in the range of ϕ_S from 1% to 3% (0.5 M to 2 M), the complex branch of the binodal phase boundary for the PAH-PAA system (depicted by blue squares) was nearly vertical, denoting little compositional change, in contrast to the strongly sloped complex branch (depicted by the red circles) for the PLK-PRE system.

Binodal phase boundaries depicted by the green diamonds and yellow triangles in **Figure 3** represent the compositions of the complex and the supernatant phases for solutions comprising polyelectrolyte pairs of PAH-PRE and PLK-PAA, respectively. The binodal boundaries for both these systems lay notably in between PAH-PAA and PLK-PRE phase boundaries. Further, both the systems exhibited "closed" binodal phase boundaries with regions of completely suppressed complexation. It is notable that in all the four pairs of polyelectrolytes considered here, the ionic groups on the oppositely charged polyelectrolytes were the same. Therefore, even though the strength of the electrostatic interactions remained the similar, the binding strength among the oppositely charged chains in the complexes that dictate the water content in the complex could be tuned by varying the chemical nature of the polyelectrolyte backbones and its affinity towards the solvent and the other polyelectrolyte present in solution.

Interactions of the polyelectrolyte backbones with the solvent and with each other were encapsulated in the effective Flory-Huggins interaction parameter χ (Equation 4). **Figure 4** shows binodal phase boundaries for polyelectrolyte complexes with systematically varying χ between 0.4 to 0.6, corresponding to the solvent conditions varying from poor solvent to good solvent. $N = 10^3$ and $f = 0.1$ were chosen to satisfy the limit of weakly charged polyelectrolytes where the RPA is rigorous and accurate. In the effectively Θ-solvent (χ = 0.5, phase boundaries shown by the green curve) PEC stability can be attributed solely to electrostatic interactions. Upon increasing salt concentration, Coulombic attractions became increasingly screened, resulting in polymer densities in the complex and the supernatant phases to approach each other readily, and eventually meeting near the critical point. In effectively good solvents for the polyelectrolytes with $\chi < 0.5$, the binodal phase boundaries, shown by red and orange curves, were smaller lower polymer density in the complex phase at comparable salt concentrations. Decreasing χ effectively led to a leftward shifting complex branch in the binodal phase maps. Correspondingly, PEC dissolution also occurred at lower salt concentrations. These transitions could be attributed to the absence of the effective short-range two-body repulsion between the monomers that exist in the effectively Θ solvent conditions (χ = 0.5).

The trends in the binodal phase boundaries were, however, very different for polyelectrolytes in effectively poor solvents (χ > 0.5). PEC stability was influenced by both (i) the electrostatic attraction between oppositely charged polyelectrolytes and (ii) the intermolecular and intramolecular short-range (hydrophobic) attractions of polyelectrolyte chains. The latter can result in formation of a dense polymer-rich phase of neutral (with strongly screened electrostatic interactions) hydrophobic polymer in poor solvent. At low salt concentrations, both factors contribute to phase separation of the polyelectrolytes, resulting in high macromolecular concentrations in the complex phase. Addition of salt caused screening of electrostatics interactions, so that, at high salt concentrations, phase separation of the polyelectrolytes in the solution, if it occurs at all, would be driven solely due to short-range hydrophobic attraction of the polymer chains. For phase separation to occur in such solutions would require a threshold χ value which corresponds to weakly poor solvent and is given by[77]

$$\chi_{cr} = \frac{1}{2}\left(1 + \frac{1}{\sqrt{N}}\right)^2 \approx \frac{1}{2} + \frac{1}{\sqrt{N}} \qquad (7)$$

Here, the $1/\sqrt{N}$ term is the contribution from the subdued translational entropy of polyelectrolyte chains. For polyelectrolytes with $N = 10^3$, $\chi_{cr} \approx 0.532$. Thus, polyelectrolytes with $\chi < \chi_{cr}$ are expected to phase separate

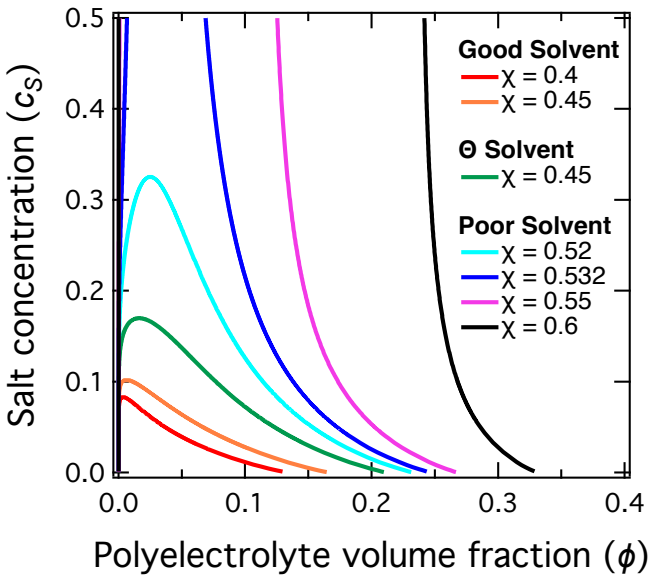

Figure 4. Polymer volume fraction (ϕ)-salt concentration (c_S) representation of the theoretical predictions of the binodal phase boundaries for polyelectrolyte complex solutions with varying hydrophobicity of polyelectrolytes governed by the effective Flory-Huggins parameter χ. Curves are plotted for $f = 0.1$, $N = 10^3$, and $u = 1$.

and form complexes that would disintegrating upon addition of appropriate amounts of salt, while polyelectrolytes with $\chi \geq \chi_{cr}$ are expected to phase separate and the resulting phases are expected to remain stable even at high salt concentrations.

The binodal phase boundaries for solutions comprising oppositely charged polyelectrolytes with effective $\chi = 0.532$ is shown in **Figure 4** with the dark blue curve. It is evident that the polymer-rich and polymer-lean branches of the binodal boundaries did not converge even at salt concentrations as high as $c_s = 0.5$. Further examination of the evolution of the binodal phase boundaries revealed intriguing features. At comparable salt concentrations, polymer content in the polymer-rich phase increased progressively with increasing χ. The binodal phase boundaries could be categorized in two regimes – systems with $\chi < \chi_{cr} = 0.532$ exhibited distinct two-phase and one-phase regions, while systems with $\chi \geq \chi_{cr}$ remained phase separated states even at the highest salt concentrations investigated here ($c_s = 0.5$). The polyelectrolyte density of complex phase gradually reduced upon salt addition at low c_s before saturating at higher c_s. These behaviors are consistent with our expectations of a transition in solution behaviors at χ_{cr}.

A comparison of our experimental observations and theoretical results, shown in **Figures 3** and **4**, respectively, highlighted broad agreements. The general shapes of binodal phase boundaries and their evolution with varying solvent quality were consistent between the experimental and theoretical treatments. The density of the complex phase increased as solvent quality became poorer, and the polymer-dense phases for polyelectrolytes with aliphatic backbones and correspondingly polyelectrolytes with $\chi \geq \chi_{cr}$ did not dissolve in high concentrations of salt. We note that stable complexes in poor solvents that persist even at high salt concentrations have been reported previously,[47,55,61,62] and our experimental and theoretical results are in general agreement with these earlier findings. We also note that while there is general agreement between our experimental and theoretical treatments, the theoretical analysis is unable to capture two key aspects of the experimental data. Theory predicted higher salt concentration within the complex phase compared with the supernatant phase, which was contrary to experiments observations of preferential salt partitioning in the polymer-lean phases in solutions comprising fully charged polyelectrolytes. This could be attributed to the assumption of weakly charged polyelectrolytes ($f \ll 1$) and point-like salt ions in the theoretical considerations. Corresponding modifications in theoretical work would require a more thorough analysis of the salt behavior within the complex phase, including excluded volume, [30,68–70,78] solvation and dielectric effects.[52] Second, the decrease in ϕ_P in the polyelectrolyte-rich phase with polyelectrolytes composed of aliphatic hydrophobic backbones at extremely high salt concentration was not reproduced in the theoretical calculations since such high salt concentration were inaccessible in the theoretical framework adopted here. RPA applicability is limited to weak Coulomb correlations, which yields $c_s \ll 1$ in aqueous solutions.[61]

IV. CONCLUSIONS

Complexed polyelectrolytes with aliphatic backbones serve as the basis of diverse materials including multifunctional membrane,[79–82] ultrafiltration,[83–85] and coatings;[86,87] understanding the role of solvent quality in their complexation would greatly improve the materials design. In this work, we provide insights on the effect of solvent quality on polyelectrolyte complexation among polyelectrolytes with nearly identical electrostatic interactions but varying solvent compatibilities. Systematic comparisons of the experimental binodal phase behaviors of four polyelectrolyte complexes with varying backbone hydrophobicity provided a route towards tuning the PEC phase behavior, compositions and salt stability. Exceptional stability of PAH-PAA complexes against NaCl addition contrasted starkly against the complete dissolution of PLK-PRE complexes at ~1 M NaCl. Corresponding theoretical considerations demonstrated complexation being driven exclusively by electrostatic attractions between charged species in good or theta solvents, while in poor solvents, backbone hydrophobicity played a vital role in dictating phase behavior leading to high salt resistances and lower water content of the resultant polymer-rich phases. This work offers a unique perspective by integrating results from multiple systems with diverse chemical structures and is expected to serve as a starting point for instructive comparison in future studies.

ASSOCIATED CONTENT

Supporting Information.

The following supporting information are available free of charge.
Turbidimetric measurements.
Microscopic images of PLK-PAA systems.

AUTHOR INFORMATION

Corresponding Authors
S. S.: samsri@ucla.edu
J. J. d. P.: depablo.uchicago.edu
M. V. T.: mtirrell@uchicago.edu

Author Contributions
L.L. S.S. and M.V.T. conceptualized the study. S.S. and L.L. designed the experiments. L.L. performed the experiments. S. M. provided microscopy assistance. A.M conducted the theoretical calculation. L.L., A.M. and S.S. contributed to the analysis/interpretation of the data and wrote the manuscript. J.J.d.P. supervised the theoretical work. S.S. and M.V.T. supervised the experimental work.

Funding Sources
This work was performed under the following financial assistance award 70NANB19H005 from U.S. Department of Commerce, National Institute of Standards and Technology (NIST) as part of the Center for Hierarchical Materials Design (CHiMaD) and MRSEC grant DMR-1420709 from U.S. National Science Foundation.

Notes
The authors declare no competing financial interests.

ACKNOWLEDGMENT
We acknowledge beneficial discussions with Jeffrey M. Ting.

ABBREVIATIONS USED
PLK: Poly(lysine) chloride salt
PRE: Poly(glutamic acid) sodium salt
PAA: Poly(acrylic acid) sodium salt
PAH: Poly(allylamine hydrochloride)
PEC: Polyelectrolyte complex
PSS: Poly(styrene sulfonate)
PDADMAC: Poly(diallyldimethylammonium chloride)
PVBTMA: Poly(vinylbenzyltrimethylammonium chloride)
PDMAEMA: Poly((2-(dimethylamino)ethyl methacrylate)
RPA: Random phase approximation

REFERENCES

(1) Kuo, C. H.; Leon, L.; Chung, E. J.; Huang, R. T.; Sontag, T. J.; Reardon, C. A.; Getz, G. S.; Tirrell, M.; Fang, Y. Inhibition of Atherosclerosis-Promoting MicroRNAs via Targeted Polyelectrolyte Complex Micelles. *J. Mater. Chem. B* **2014**, *2* (46), 8142–8153. https://doi.org/10.1039/c4tb00977k.

(2) Lee, S. H.; Mok, H.; Lee, Y.; Park, T. G. Self-Assembled SiRNA-PLGA Conjugate Micelles for Gene Silencing. *J. Control. Release* **2011**, *152* (1), 152–158. https://doi.org/10.1016/j.jconrel.2010.12.007.

(3) Bae, K. H.; Moon, C. W.; Lee, Y.; Park, T. G. Intracellular Delivery of Heparin Complexed with Chitosan-g-Poly(Ethylene Glycol) for Inducing Apoptosis. *Pharm. Res.* **2009**, *26* (1), 93–100. https://doi.org/10.1007/s11095-008-9713-1.

(4) Lindhoud, S.; De Vries, R.; Schweins, R.; Cohen Stuart, M. A.; Norde, W. Salt-Induced Release of Lipase from Polyelectrolyte Complex Micelles. *Soft Matter* **2009**, *5* (1), 242–250. https://doi.org/10.1039/b811640g.

(5) Zhao, Q.; Lee, D. W.; Ahn, B. K.; Seo, S.; Kaufman, Y.; Israelachvili, J. N.; Waite, J. H. Underwater Contact Adhesion and Microarchitecture in Polyelectrolyte Complexes Actuated by Solvent Exchange. *Nat. Mater.* **2016**, *15* (4), 407–412. https://doi.org/10.1038/nmat4539.

(6) Shao, H.; Stewart, R. J. Biomimetic Underwater Adhesives with Environmentally Triggered Setting Mechanisms. *Adv. Mater.* **2010**, *22* (6), 729–733. https://doi.org/10.1002/adma.200902380.

(7) Aumiller, W. M.; Pir Cakmak, F.; Davis, B. W.; Keating, C. D. RNA-Based Coacervates as a Model for Membraneless Organelles: Formation, Properties, and Interfacial Liposome Assembly. *Langmuir* **2016**, *32* (39), 10042–10053. https://doi.org/10.1021/acs.langmuir.6b02499.

(8) Brangwynne, C. P.; Tompa, P.; Pappu, R. V. Polymer Physics of Intracellular Phase Transitions. *Nat. Phys.* **2015**, *11* (11), 899–904. https://doi.org/10.1038/nphys3532.

(9) Fu, J.; Schlenoff, J. B. Driving Forces for Oppositely Charged Polyion Association in Aqueous Solutions: Enthalpic, Entropic, but Not Electrostatic. *J. Am. Chem. Soc.* **2016**, *138* (3), 980–990. https://doi.org/10.1021/jacs.5b11878.

(10) Priftis, D.; Laugel, N.; Tirrell, M. Thermodynamic Characterization of Polypeptide Complex Coacervation. *Langmuir* **2012**, *28* (45), 15947–15957. https://doi.org/10.1021/la302729r.

(11) Vitorazi, L.; Ould-Moussa, N.; Sekar, S.; Fresnais, J.; Loh, W.; Chapel, J. P.; Berret, J. F. Evidence of a Two-Step Process and Pathway Dependency in the Thermodynamics of Poly(Diallyldimethylammonium Chloride)/Poly(Sodium Acrylate) Complexation. *Soft Matter* **2014**, *10* (47), 9496–9505. https://doi.org/10.1039/c4sm01461h.

(12) Li, L.; Srivastava, S.; Andreev, M.; Marciel, A. B.; De Pablo, J. J.; Tirrell, M. V. Phase Behavior and Salt Partitioning in Polyelectrolyte Complex Coacervates. *Macromolecules* **2018**, *51* (8), 2988–2995. https://doi.org/10.1021/acs.macromol.8b00238.

(13) Priftis, D.; Tirrell, M. Phase Behaviour and Complex Coacervation of Aqueous Polypeptide Solutions. *Soft Matter* **2012**, *8* (36), 9396–9405.

https://doi.org/10.1039/c2sm25604e.
(14) Srivastava, S.; Andreev, M.; Levi, A. E.; Goldfeld, D. J.; Mao, J.; Heller, W. T.; Prabhu, V. M.; De Pablo, J. J.; Tirrell, M. V. Gel Phase Formation in Dilute Triblock Copolyelectrolyte Complexes. *Nat. Commun.* **2017**, *8*, 1–9. https://doi.org/10.1038/ncomms14131.
(15) Wang, Q.; Schlenoff, J. B. The Polyelectrolyte Complex/Coacervate Continuum. *Macromolecules* **2014**, *47* (9), 3108–3116. https://doi.org/10.1021/ma500500q.
(16) Zhang, Y.; Yildirim, E.; Antila, H. S.; Valenzuela, L. D.; Sammalkorpi, M.; Lutkenhaus, J. L. The Influence of Ionic Strength and Mixing Ratio on the Colloidal Stability of PDAC/PSS Polyelectrolyte Complexes. *Soft Matter* **2015**, *11* (37), 7392–7401. https://doi.org/10.1039/c5sm01184a.
(17) Tirrell, M. Polyelectrolyte Complexes: Fluid or Solid? *ACS Cent. Sci.* **2018**, *4* (5), 532–533. https://doi.org/10.1021/acscentsci.8b00284.
(18) Krogstad, D. V.; Lynd, N. A.; Miyajima, D.; Gopez, J.; Hawker, C. J.; Kramer, E. J.; Tirrell, M. V. Structural Evolution of Polyelectrolyte Complex Core Micelles and Ordered-Phase Bulk Materials. *Macromolecules* **2014**, *47* (22), 8026–8032. https://doi.org/10.1021/ma5017852.
(19) Reisch, A.; Roger, E.; Phoeung, T.; Antheaume, C.; Orthlieb, C.; Boulmedais, F.; Lavalle, P.; Schlenoff, J. B.; Frisch, B.; Schaaf, P. On the Benefits of Rubbing Salt in the Cut: Self-Healing of Saloplastic PAA/PAH Compact Polyelectrolyte Complexes. *Adv. Mater.* **2014**, *26* (16), 2547–2551. https://doi.org/10.1002/adma.201304991.
(20) Sadman, K.; Wang, Q.; Chen, Y.; Keshavarz, B.; Jiang, Z.; Shull, K. R. Influence of Hydrophobicity on Polyelectrolyte Complexation. *Macromolecules* **2017**, *50* (23), 9417–9426. https://doi.org/10.1021/acs.macromol.7b02031.
(21) Spruijt, E.; Sprakel, J.; Lemmers, M.; Stuart, M. A. C.; Van Der Gucht, J. Relaxation Dynamics at Different Time Scales in Electrostatic Complexes: Time-Salt Superposition. *Phys. Rev. Lett.* **2010**, *105* (20), 1–4. https://doi.org/10.1103/PhysRevLett.105.208301.
(22) Veis, A. A Review of the Early Development of the Thermodynamics of the Complex Coacervation Phase Separation. *Adv. Colloid Interface Sci.* **2011**, *167* (1–2), 2–11. https://doi.org/10.1016/j.cis.2011.01.007.
(23) Veis, A.; Aranyi, C. Phase Separation in Polyelectrolyte Systems. I. Complex Coacervates of Gelatin. *J. Phys. Chem.* **1960**, *64* (9), 1203–1210. https://doi.org/10.1021/j100838a022.
(24) Arthur, V.; Edward, B.; Shirley, M. Molecular Weight Fractionation and the Self-suppression of Complex Coacervation. *Biopolymers* **1967**, *5* (1), 37–59.
(25) Ting, J. M.; Wu, H.; Herzog-Arbeitman, A.; Srivastava, S.; Tirrell, M. V. Synthesis and Assembly of Designer Styrenic Diblock Polyelectrolytes. *ACS Macro Lett.* **2018**, *7* (6), 726–733. https://doi.org/10.1021/acsmacrolett.8b00346.
(26) Spruijt, E.; Westphal, A. H.; Borst, J. W.; Cohen Stuart, M. A.; Van Der Gucht, J. Binodal Compositions of Polyelectrolyte Complexes. *Macromolecules* **2010**, *43* (15), 6476–6484. https://doi.org/10.1021/ma101031t.
(27) Borue, V. Y.; Erukhimovich, I. Y. A Statistical Theory of Globular Polyelectrolyte Complexes. *Macromolecules* **1990**, *23* (15), 3625–3632. https://doi.org/10.1021/ma00217a015.
(28) Shusharina, N. P.; Zhulina, E. B.; Dobrynin, A. V.; Rubinstein, M. Scaling Theory of Diblock Polyampholyte Solutions. *Macromolecules* **2005**, *38* (21), 8870–8881. https://doi.org/10.1021/ma051324g.
(29) Lee, J.; Popov, Y. O.; Fredrickson, G. H. Complex Coacervation: A Field Theoretic Simulation Study of Polyelectrolyte Complexation. *J. Chem. Phys.* **2008**, *128* (22). https://doi.org/10.1063/1.2936834.
(30) Perry, S. L.; Sing, C. E. PRISM-Based Theory of Complex Coacervation: Excluded Volume versus Chain Correlation. *Macromolecules* **2015**, *48* (14), 5040–5053. https://doi.org/10.1021/acs.macromol.5b01027.
(31) Ou, Z.; Muthukumar, M. Entropy and Enthalpy of Polyelectrolyte Complexation: Langevin Dynamics Simulations. *J. Chem. Phys.* **2006**, *124* (15). https://doi.org/10.1063/1.2178803.
(32) Chang, L. W.; Lytle, T. K.; Radhakrishna, M.; Madinya, J. J.; Vélez, J.; Sing, C. E.; Perry, S. L. Sequence and Entropy-Based Control of Complex Coacervates. *Nat. Commun.* **2017**, *8* (1), 1–7. https://doi.org/10.1038/s41467-017-01249-1.
(33) Diddens, D.; Baschnagel, J.; Johner, A. Microscopic Structure of Compacted Polyelectrolyte Complexes: Insights from Molecular Dynamics Simulations. *ACS Macro Lett.* **2019**, *8* (2), 123–127. https://doi.org/10.1021/acsmacrolett.8b00630.
(34) Gucht, J. van der; Spruijt, E.; Lemmers, M.; Cohen Stuart, M. A. Polyelectrolyte Complexes: Bulk Phases and Colloidal Systems. *J. Colloid Interface Sci.* **2011**, *361* (2), 407–422. https://doi.org/10.1016/j.jcis.2011.05.080.
(35) Srivastava, S.; Tirrell, M. V. POLYELECTROLYTE COMPLEXATION. *Adv. Chem. Phys.* **2016**, *161*, 499–544.
(36) Sing, C. E. Development of the Modern Theory of Polymeric Complex Coacervation. *Adv. Colloid Interface Sci.* **2017**, *239*, 2–16. https://doi.org/10.1016/j.cis.2016.04.004.
(37) Sing, C. E.; Perry, S. L. Recent Progress in the Science of Complex Coacervation. *Soft Matter* **2020**, 2885–2914. https://doi.org/10.1039/d0sm00001a.
(38) Fu, J.; Fares, H. M.; Schlenoff, J. B. Ion-Pairing Strength in Polyelectrolyte Complexes. *Macromolecules* **2017**, *50* (3), 1066–1074.
(39) Zhang, Y.; Li, F.; Valenzuela, L. D.; Sammalkorpi, M.; Lutkenhaus, J. L. Effect of Water on the Thermal Transition Observed in Poly(Allylamine

Hydrochloride)-Poly(Acrylic Acid) Complexes. *Macromolecules* **2016**, *49* (19), 7563–7570.

(40) Vieregg, J. R.; Lueckheide, M.; Marciel, A. B.; Leon, L.; Bologna, A. J.; Rivera, J. R.; Tirrell, M. V. Oligonucleotide-Peptide Complexes: Phase Control by Hybridization. *J. Am. Chem. Soc.* **2018**, *140* (5), 1632–1638. https://doi.org/10.1021/jacs.7b03567.

(41) Priftis, D.; Leon, L.; Song, Z.; Perry, S. L.; Margossian, K. O.; Tropnikova, A.; Cheng, J.; Tirrell, M. Self-Assembly of α-Helical Polypeptides Driven by Complex Coacervation. *Angew. Chemie - Int. Ed.* **2015**, *54* (38), 11128–11132.

(42) Priftis, D.; Xia, X.; Margossian, K. O.; Perry, S. L.; Leon, L.; Qin, J.; De Pablo, J. J.; Tirrell, M. Ternary, Tunable Polyelectrolyte Complex Fluids Driven by Complex Coacervation. *Macromolecules* **2014**, *47* (9), 3076–3085.

(43) Chollakup, R.; Smitthipong, W.; Eisenbach, C. D.; Tirrell, M. Phase Behavior and Coacervation of Aqueous Poly(Acrylic Acid)-Poly(Allylamine) Solutions. *Macromolecules* **2010**, *43* (5), 2518–2528. https://doi.org/10.1021/ma902144k.

(44) Perry, S. L.; Li, Y.; Priftis, D.; Leon, L.; Tirrell, M. The Effect of Salt on the Complex Coacervation of Vinyl Polyelectrolytes. *Polymers (Basel).* **2014**, *6* (6), 1756–1772. https://doi.org/10.3390/polym6061756.

(45) Chang, L. W.; Lytle, T. K.; Radhakrishna, M.; Madinya, J. J.; Vélez, J.; Sing, C. E.; Perry, S. L. Sequence and Entropy-Based Control of Complex Coacervates. *Nat. Commun.* **2017**, *8*, 1273.

(46) Salehi, A.; Desai, P. S.; Li, J.; Steele, C. A.; Larson, R. G. Relationship between Polyelectrolyte Bulk Complexation and Kinetics of Their Layer-by-Layer Assembly. *Macromolecules* **2015**, *48* (2), 400–409.

(47) Jha, P. K.; Desai, P. S.; Li, J.; Larson, R. G. PH and Salt Effects on the Associative Phase Separation of Oppositely Charged Polyelectrolytes. *Polymers (Basel).* **2014**, *6* (5), 1414–1436. https://doi.org/10.3390/polym6051414.

(48) Overbeek, J. T. G.; Voorn, M. J. Phase Separation in Polyelectrolyte Solutions. Theory of Complex Coacervation. *J. Cell. Comp. Physiol.* **1961**, *49*, 7–26.

(49) Nakajima, A.; Sato, H. Phase Relationships of an Equivalent Mixture of Sulfated Polyvinyl Alcohol and Aminoacetalyzed Polyvinyl Alcohol in Microsalt Aqueous Solution. *Biopolymers* **1972**, *11* (7), 1345–1355. https://doi.org/10.1002/bip.1972.360110704.

(50) Sato, H.; Nakajima, A. Complex Coacervation in Sulfated Polyvinyl Alcohol - Aminoacetalyzed Polyvinyl Alcohol System. *Polymer (Guildf).* **1974**, *948*, 944–948.

(51) Li, L.; Srivastava, S.; Meng, S.; Ting, J. M.; Tirrell, M. V. The Effect of Non-Electrostatic Intermolecular Interactions in the Phase Behavior of pH-Sensitive Polyelectrolyte Complexes. *Submitted to Macromolecules*.

(52) Salehi, A.; Larson, R. G. A Molecular Thermodynamic Model of Complexation in Mixtures of Oppositely Charged Polyelectrolytes with Explicit Account of Charge Association/Dissociation. *Macromolecules* **2016**, *49* (24), 9706–9719. https://doi.org/10.1021/acs.macromol.6b01464.

(53) Kudlay, A.; Ermoshkin, A. V.; De La Cruz, M. O. Complexation of Oppositely Charged Polyelectrolytes: Effect of Ion Pair Formation. *Macromolecules* **2004**, *37* (24), 9231–9241. https://doi.org/10.1021/ma048519t.

(54) Castelnovo, M.; Joanny, J. F. Formation of Polyelectrolyte Multilayers. *Langmuir* **2000**, *16* (19), 7524–7532. https://doi.org/10.1021/la000211h.

(55) Kudlay, A.; De la Cruz, M. O. Precipitation of Oppositely Charged Polyelectrolytes in Salt Solutions. *J. Chem. Phys.* **2004**, *120* (1), 404–412. https://doi.org/10.1063/1.1629271.

(56) Oskolkov, N. N.; Potemkin, I. I. Complexation in Asymmetric Solutions of Oppositely Charged Polyelectrolytes: Phase Diagram. *Macromolecules* **2007**, *40* (23), 8423–8429. https://doi.org/10.1021/ma0709304.

(57) Potemkin, I. I.; Palyulin, V. V. Complexation of Oppositely Charged Polyelectrolytes: Effect of Discrete Charge Distribution along the Chain. *Phys. Rev. E - Stat. Nonlinear, Soft Matter Phys.* **2010**, *81* (4), 1–6. https://doi.org/10.1103/PhysRevE.81.041802.

(58) Qin, J.; De Pablo, J. J. Criticality and Connectivity in Macromolecular Charge Complexation. *Macromolecules* **2016**, *49* (22), 8789–8800. https://doi.org/10.1021/acs.macromol.6b02113.

(59) Rumyantsev, A. M.; De Pablo, J. J. Liquid Crystalline and Isotropic Coacervates of Semiflexible Polyanions and Flexible Polycations. *Macromolecules* **2019**, *52* (14), 5140–5156. https://doi.org/10.1021/acs.macromol.9b00797.

(60) Rumyantsev, A. M.; Jackson, N. E.; Yu, B.; Ting, J. M.; Chen, W.; Tirrell, M. V.; De Pablo, J. J. Controlling Complex Coacervation via Random Polyelectrolyte Sequences. *ACS Macro Lett.* **2019**, *8* (10), 1296–1302. https://doi.org/10.1021/acsmacrolett.9b00494.

(61) Rumyantsev, A. M.; Zhulina, E. B.; Borisov, O. V. Complex Coacervate of Weakly Charged Polyelectrolytes: Diagram of States. *Macromolecules* **2018**, *51* (10), 3788–3801. https://doi.org/10.1021/acs.macromol.8b00342.

(62) Rumyantsev, A. M.; Kramarenko, E. Y.; Borisov, O. V. Microphase Separation in Complex Coacervate Due to Incompatibility between Polyanion and Polycation. *Macromolecules* **2018**, *51* (17), 6587–6601. https://doi.org/10.1021/acs.macromol.8b00721.

(63) Delaney, K. T.; Fredrickson, G. H. Theory of Polyelectrolyte Complexation - Complex Coacervates Are Self-Coacervates. *J. Chem. Phys.* **2017**, *146* (22). https://doi.org/10.1063/1.4985568.

(64) Danielsen, S. P. O.; McCarty, J.; Shea, J. E.; Delaney, K. T.; Fredrickson, G. H. Molecular Design of Self-Coacervation Phenomena in Block Polyampholytes. *Proc. Natl. Acad. Sci. U. S. A.* **2019**, *116* (17), 8224–8232. https://doi.org/10.1073/pnas.1900435116.

(65) McCarty, J.; Delaney, K. T.; Danielsen, S. P. O.; Fredrickson, G. H.; Shea, J. E. Complete Phase Diagram for Liquid-Liquid Phase Separation of Intrinsically Disordered Proteins. *J. Phys. Chem. Lett.* **2019**, *10* (8), 1644–1652. https://doi.org/10.1021/acs.jpclett.9b00099.

(66) Rumyantsev, A. M.; Potemkin, I. I. Explicit Description of Complexation between Oppositely Charged Polyelectrolytes as an Advantage of the Random Phase Approximation over the Scaling Approach. *Phys. Chem. Chem. Phys.* **2017**, *19* (40), 27580–27592. https://doi.org/10.1039/c7cp05300b.

(67) Landau, L. D.; Lifshitz, E. M. *Statistical Physics, Part 1; Pergamon Press: New York, 1970*.

(68) Lytle, T. K.; Sing, C. E. Transfer Matrix Theory of Polymer Complex Coacervation. *Soft Matter* **2017**, *13* (39), 7001–7012. https://doi.org/10.1039/c7sm01080j.

(69) Zhang, P.; Alsaifi, N. M.; Wu, J.; Wang, Z. G. Salting-Out and Salting-In of Polyelectrolyte Solutions: A Liquid-State Theory Study. *Macromolecules* **2016**, *49* (24), 9720–9730. https://doi.org/10.1021/acs.macromol.6b02160.

(70) Zhang, P.; Shen, K.; Alsaifi, N. M.; Wang, Z. G. Salt Partitioning in Complex Coacervation of Symmetric Polyelectrolytes. *Macromolecules* **2018**, *51* (15), 5586–5593.

(71) Zhang, P.; Alsaifi, N. M.; Wu, J.; Wang, Z. G. Polyelectrolyte Complex Coacervation: Effects of Concentration Asymmetry. *J. Chem. Phys.* **2018**, *149* (16). https://doi.org/10.1063/1.5028524.

(72) Zhang, Y.; Batys, P.; O'Neal, J. T.; Li, F.; Sammalkorpi, M.; Lutkenhaus, J. L. Molecular Origin of the Glass Transition in Polyelectrolyte Assemblies. *ACS Cent. Sci.* **2018**, *4* (5), 638–644. https://doi.org/10.1021/acscentsci.8b00137.

(73) Fares, H. M.; Wang, Q.; Yang, M.; Schlenoff, J. B. Swelling and Inflation in Polyelectrolyte Complexes. *Macromolecules* **2019**, *52* (2), 610–619. https://doi.org/10.1021/acs.macromol.8b01838.

(74) Shen, K.; Wang, Z. G. Polyelectrolyte Chain Structure and Solution Phase Behavior. *Macromolecules* **2018**, *51* (5), 1706–1717. https://doi.org/10.1021/acs.macromol.7b02685.

(75) Rubinstein, M.; Liao, Q.; Panyukov, S. Structure of Liquid Coacervates Formed by Oppositely Charged Polyelectrolytes. *Macromolecules* **2018**, *51* (23), 9572–9588. https://doi.org/10.1021/acs.macromol.8b02059.

(76) Perry, S. L.; Leon, L.; Hoffmann, K. Q.; Kade, M. J.; Priftis, D.; Black, K. A.; Wong, D.; Klein, R. A.; Pierce, C. F.; Margossian, K. O.; et al. Chirality-Selected Phase Behaviour in Ionic Polypeptide Complexes. *Nat. Commun.* **2015**, *6*. https://doi.org/10.1038/ncomms7052.

(77) Rubinstein, M.; Colby, R. H. *Polymer Physics*; 2003. https://doi.org/10.1145/2024288.2024304.

(78) Lytle, T. K.; Chang, L. W.; Markiewicz, N.; Perry, S. L.; Sing, C. E. Designing Electrostatic Interactions via Polyelectrolyte Monomer Sequence. *ACS Cent. Sci.* **2019**, *5* (4), 709–718. https://doi.org/10.1021/acscentsci.9b00087.

(79) Schönhoff, M.; Bieker, P. Linear and Exponential Growth Regimes of Multilayers of Weak Polyelectrolytes in Dependence on PH. *Macromolecules* **2010**, *43* (11), 5052–5059. https://doi.org/10.1021/ma1007489.

(80) Kelly, K. D.; Schlenoff, J. B. Spin-Coated Polyelectrolyte Coacervate Films. *ACS Appl. Mater. Interfaces* **2015**, *7* (25), 13980–13986. https://doi.org/10.1021/acsami.5b02988.

(81) Shan, L.; Guo, H.; Qin, Z.; Wang, N.; Ji, S.; Zhang, G.; Zhang, Z. Covalent Crosslinked Polyelectrolyte Complex Membrane with High Negative Charges towards Anti-Natural Organic Matter Fouling Nanofiltration. *RSC Adv.* **2015**, *5* (15), 11515–11523.

(82) Boas, M.; Gradys, A.; Vasilyev, G.; Burman, M.; Zussman, E. Electrospinning Polyelectrolyte Complexes: PH-Responsive Fibers. *Soft Matter* **2015**, *11* (9), 1739–1747. https://doi.org/10.1039/c4sm02618g.

(83) Musale, D. A.; Kumar, A.; Pleizier, G. Formation and Characterization of Poly (Acrylonitrile)/ Chitosan Composite Ultrafiltration Membranes. *J. Memb. Sci.* **1999**, *154*, 163–173.

(84) Guo, W.; Uchiyama, H.; Tucker, E. E.; Christian, S. E.; Scamehorn, J. F. Use of Polyelectrolyte-Surfactant Complexes in Colloid-Enhanced Ultrafiltration. *Colloids and Surfaces* **1997**, *123–124*, 695–703.

(85) Zhang, G.; Yan, H.; Ji, S.; Liu, Z. Self-Assembly of Polyelectrolyte Multilayer Pervaporation Membranes by a Dynamic Layer-by-Layer Technique on a Hydrolyzed Polyacrylonitrile Ultrafiltration Membrane. *J. Memb. Sci.* **2007**, *292* (1–2), 1–8. https://doi.org/10.1016/j.memsci.2006.11.023.

(86) Müller, M.; Rieser, T.; Lunkwitz, K.; Meier-Haack, J. Polyelectrolyte Complex Layers: A Promising Concept for Antifouling Coatings Verified by in-Situ ATR-FTIR Spectroscopy. *Macromol. Rapid Commun.* **1999**, *20* (12), 607–611. https://doi.org/10.1002/(SICI)1521-3927(19991201)20:12<607::AID-MARC607>3.0.CO;2-Z.

(87) Bertrand, P.; Jonas, A.; Laschewsky, A.; Legras, R. Ultrathin Polymer Coatings by Complexation of Polyelectrolytes at Interfaces: Suitable Materials, Structure and Properties. *Macromol. Rapid Commun.* **2000**, *21* (7), 319–348. https://doi.org/10.1002/(SICI)1521-3927(20000401)21:7<319::AID-MARC319>3.0.CO;2-7.

Table of Contents Figure